

# Neutrino yield and neutron shielding calculations for a high-power target installed in an underground setting

Adriana Bungau, Jose Alonso, Roger Barlow, Larry Bartoszsek, Janet Conrad, Michael Shaevitz, Joshua Spitz, and Daniel Winklehner

**Abstract**—With the ever increasing beam power at particle accelerator-based facilities for nuclear and particle physics, radioactive isotope production, and nuclear engineering, targets that can withstand this power, and shielding of secondary particles are becoming increasingly important. Here we present Monte Carlo (MC) calculations using the well-established Geant4 software to optimise and predict the antineutrino yield of a  $^8\text{Li}$  Decay-At-Rest (DAR) source. The source relies on 600 kW of beam power from a continuous wave proton beam impinging on a beryllium target, where spallation neutrons capture on  $^7\text{Li}$  to produce the  $^8\text{Li}$ . We further present an in-depth treatment of the neutron shielding surrounding this target. We show that we can produce the high antineutrino flux needed for the discovery-level experiment IsoDAR, searching for “sterile” neutrinos (predicted new fundamental particles) and other beyond standard model physics, while maintaining a neutron flux in the detector that is below natural backgrounds. The methods presented in this paper are easily transferable to other high-power targets and their associated shielding.

## I. INTRODUCTION

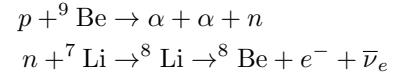
Underground laboratories provide areas of exceedingly low background for very sensitive experiments. Placing these experiments in caverns with typically a thousand meters of rock overburden reduces the cosmic muon flux by a factor of several million compared to the rate at the surface. An experiment such as IsoDAR [1], [2], which is designed to place an intense source of neutrinos in close proximity to a large liquid scintillation detector, produces locally extremely high levels of radiation and neutrons, a necessary consequence of the reactions needed to produce the desired neutrino flux.

This poses the question whether it is possible to deploy such a neutrino production facility in an underground laboratory while maintaining the quiet environment for other experiments in the same facility. The answer is yes, but it must be done with careful attention to shielding, regulatory requirements, and containment of all sources of radiation and neutrons.

Strategies for achieving this have been presented in several preceding papers [3]–[5], which addressed the deployment of

IsoDAR at the Kamioka Observatory, in close proximity to the KamLAND liquid scintillation detector. The present work focuses on a new site, Yemilab, in South Korea, and presents designs appropriate for this site and the planned LSC 2.4 kiloton liquid scintillator detector. More importantly, this paper addresses considerations and general techniques that should be employed in matching such a high-radiation source with the clean and low-background underground environment.

The IsoDAR experiment will use a 60 MeV, 10 mA proton beam, produced by a novel compact cyclotron [6], [7], directed onto a  $^9\text{Be}$  target to produce neutrons, which enter a sleeve of  $^7\text{Li}$  to produce  $^8\text{Li}$ . The  $^8\text{Li}$  rapidly  $\beta$  decays ( $t_{1/2} = 0.839$  s) to provide a source of electron antineutrinos ( $\bar{\nu}_e$ ):



The  $\bar{\nu}_e$  can be detected through inverse beta decay (IBD),  $\bar{\nu}_e + p \rightarrow e^+ + n$ , in a large liquid scintillator detector (e.g., the LSC at Yemilab [8]) enabling precision studies of neutrino oscillations, that will definitively elucidate the hints (from, e.g., radioactive-source-based [9]–[11] and accelerator-based short baseline neutrino experiments [12], [13]) possibly indicating the existence of “sterile” neutrinos, and allow a range of other beyond-standard-model (BSM) physics searches [1], [14], [15]. The proposed design calls for five years of running, giving a data sample of approximately 1.67 million selected IBD events. This requires the production of  $4.6 \times 10^{15}$  antineutrinos/second. Optimising this number requires careful consideration of the target composition and geometry, and this study is the first topic of this paper. The

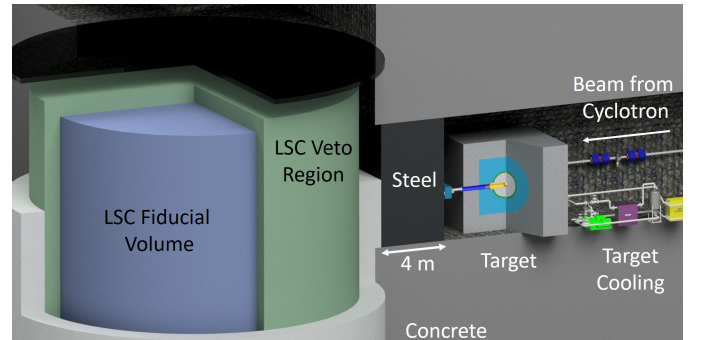


Fig. 1. The layout of the IsoDAR target and the LSC detector at Yemilab [8].

Jose Alonso, Adriana Bungau, Janet Conrad and Daniel Winklehner are with Massachusetts Institute of Technology, 77 Massachusetts Ave, Cambridge, MA 02139, USA

Roger Barlow is with the University of Huddersfield, Huddersfield HD1 3DH, UK

Larry Bartoszsek is with Bartoszsek Engineering, Aurora IL, USA

Michael Shaevitz is with Columbia University, New York, New York 10027, USA

Joshua Spitz is with the University of Michigan, Ann Arbor, Michigan 48109, USA

second topic is neutron shielding; the flux within the target is, by design, extremely high and shielding is required to screen the surroundings, both for reasons of safety and to avoid backgrounds in the LSC where a  $\gtrsim 3$  MeV neutron can produce a signal similar to an IBD event. These topics were considered in two previous publications [4], [5]. An update is necessary for several reasons.

- 1) The target has been redesigned to have three hemispherical beryllium shells rather than a simple disc, for relieving unacceptably high thermal stresses at the edges of the original flat target.
- 2) The shape and dimensions of the surrounding lithium-beryllium sleeve have been optimised to maximise antineutrino production with the most efficient utilization of the highly-enriched  $^7\text{Li}$  inventory.
- 3) The Geant4 ‘Shielding’ package has become available [16], enabling many of the relevant simulations to be done more quickly and accurately; for lower neutron energies the Shielding package uses the high-precision (HP) neutron package which includes the available evaluated neutron data for neutron interactions below 20 MeV. For energies above 20 MeV the Bertini cascade inelastic scattering model [17] is used for energies up to 3 GeV along with the JENDL HE-2007 neutron cross sections available at these higher energies; a direct Geant4-MCNP shielding comparison study has already been done and it has shown very good agreements between the two codes [18]; the Geant4 Shielding package is being used in all the shielding aspects of accelerator, target and irradiation facilities workshops [19] since 2002 as part of the ‘Intercomparison of Medium-energy Neutron Attenuation in Iron and Concrete’ project [20].
- 4) The previous accounts considered only the KamLAND site; here, we address Yemilab-specific issues, however the methods employed can be applied to the requirements of any specific site.
- 5) Various other relevant studies have been done in response to questions that have arisen.

The general layout of the experiment is shown in Figure 1. The beam from the cyclotron (off the figure to the right, in an existing cavern specifically constructed for it by the Yemilab Laboratory) is bent through  $180^\circ$  before striking the target. This geometry was chosen to give space to enable the target assembly to be withdrawn and replaced, which we anticipate will be necessary several times during the lifetime of the experiment. It has the additional benefit of reducing the background from high energy neutrons directed towards the detector, as will be discussed later (see Fig. 9). The LSC is shielded from the target by steel and concrete: the thickness of these layers is an important design choice, as increasing the thickness reduces the neutron background but also the antineutrino signal (since the antineutrino yield is isotropic, increasing shielding increases the distance from the detector, and the flux drops as  $1/r^2$ ).

The IsoDAR target design presented in Ref. [5] and updated in Ref. [3] has been redesigned, as shown in Figure 2.

At the vacuum interface, the proton beam impinges on a

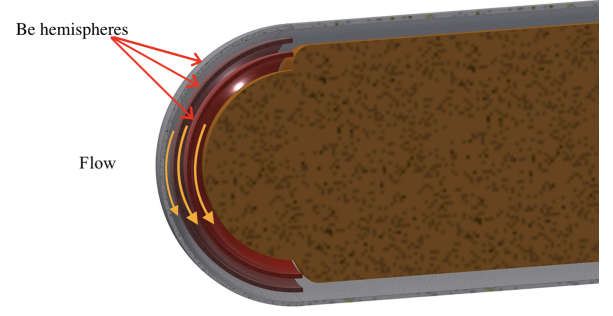


Fig. 2. The target: beryllium shells and cooling heavy water.

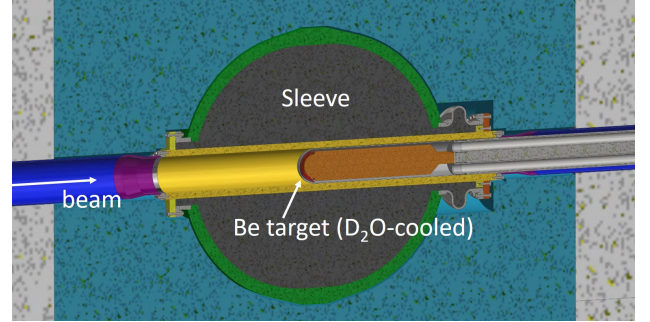


Fig. 3. The target surrounded by the Li-Be sleeve.

3 mm thick hemispherical beryllium shell. Behind it lie two more concentric, 3 mm thick, beryllium shells separated by 2 mm deep channels of heavy water. Finally, the centre is comprised of a solid beryllium block. Full details, including strategies to avoid stopping of protons in beryllium layers of the target, which is known to lead to embrittlement because of poor solubility of hydrogen in beryllium [21], are given in an upcoming publication on the mechanical design and fluid dynamics of the target and cooling.

The cylindrical Li/Be sleeve of the previous design has been replaced by a (roughly) spherical section, as shown in Figure 3, following the optimisation analysis developed in [5].

## II. METHODS

To simulate all stages of the process we use the Geant4 library [22]. Originally developed for the description of particle physics detectors, it has since been expanded and applied to many fields. We use version Geant4-11.0.2. The shielding physics list was used for the shielding calculations, and the binary cascade and QGSP options are used for the reactions relevant to antineutrino production. The ‘high precision’ cross section libraries for neutron interactions are included, as these processes turn out to have an important contribution.

In order to maximise the production of antineutrinos we must maximise that of the precursor neutrons. The disintegration of  $^9\text{Be}$  was the method by which the neutron was first seen [23] and is still the most efficient way of producing neutrons using a small accelerator. (Lithium also gives neutrons, but is structurally unworkable, with a low melting point.)

The target constitutes a very high intensity neutron source, and shielding must be put in place to attenuate these pene-

trating particles beyond the production sleeve. The IsoDAR experiment will be deep underground and will be controlled remotely, so exposure of personnel is not an issue. Components will become activated, but maintenance work will be possible after a suitable cooling-off period. The two principal concerns are for the activation in the surrounding rock, which must remain below a statutorily-required level (discussed later) on completion of the experiment, and backgrounds in the LSC detector, where a high energy neutron interaction, with possible subsequent capture, can mimic the signature of an antineutrino event.

The shielding materials considered were:

- Iron, which has a high interaction cross section for high energy neutrons (above  $\sim 2$  MeV).
- Boron loaded concrete, which has a high absorption cross section for slow neutrons.

A typical configuration considered was a thick layer of iron, which slowed down the fast neutrons, followed by a layer of boron loaded concrete to remove the resulting slow neutrons. Gadolinium loaded polyethylene was also considered since it has properties similar to Boron loaded concrete.

Considering the background in the detector, low energy neutrons below  $\sim 3$  MeV are not a problem as they do not resemble the signal from an antineutrino-induced IBD or elastic scattering event, so the second shielding layer is not necessary for this purpose.

### III. RESULTS

#### A. Neutron and antineutrino yield

The new IsoDAR design features a hemispherical beryllium target, as described in Section I.

Neutrons are produced both in the beryllium shells and in the heavy water between them. A pure heavy water target was considered, but even after optimisation this could produce only half as many neutrons as the beryllium. Similarly, cooling with light water produces a significantly lower yield of neutrons.

The target is surrounded by a sleeve, as shown in Figure 3. This contains lithium ( ${}^7\text{Li}$ ), from which the desired  ${}^8\text{Li}$  is formed, and also beryllium, as this multiplies the neutron flux through the  $(n, 2n)$  multiplicative reaction.

The previous design [5] used a cylindrical sleeve, but simulations showed that the neutron production was, as one would expect, roughly spherical, and so the amount of expensive sleeve material can be reduced by removing the least productive volumes. The optimised radius is 75 cm and the length 110 cm, so it is an ellipsoid rather than a sphere (though for some simulations a sphere is used for simplicity).

The previous design studies [5] showed that the optimum sleeve material was a mixture of beryllium and isotopically pure  ${}^7\text{Li}$ , with a Be mass fraction of 75%. It is formed of 1 mm diameter beryllium spheres in lithium. A FLiBe eutectic mix was also considered, but is less performant [5].

The previous design achieved a production rate of 0.018  ${}^8\text{Li}$  per incident proton. The new nested-shell target design, necessary for cooling, initially reduced this by a factor  $\sim 4$ . This figure, which is a key measure of performance, has been increased again by optimisation of the target and sleeve

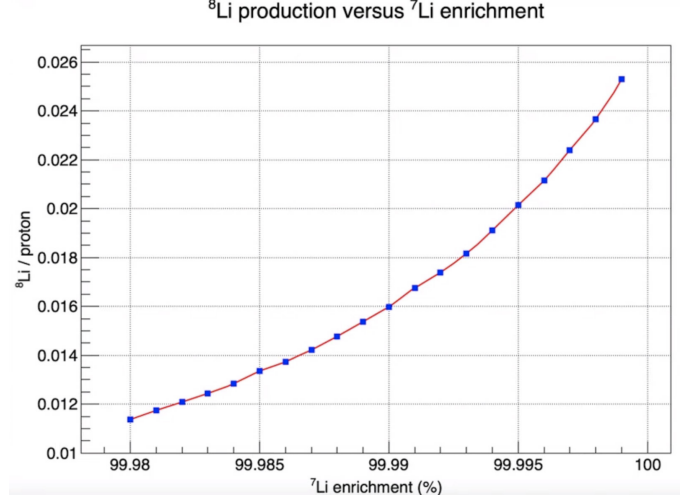


Fig. 4.  ${}^8\text{Li}$  production as a function of  ${}^7\text{Li}$  enrichment.

geometry, and by increasing the isotopic purity of the lithium.  ${}^6\text{Li}$  has a very large neutron cross section, and even small amounts will have a serious negative effect. Natural lithium is 92.5% pure  ${}^7\text{Li}$ , and we need this to be increased to well over 99%, as shown in Figure 4. A purity of 99.99% will give 0.016  ${}^8\text{Li}$  per proton, which is sufficient for the experiment, and 99.995% will give 0.020. A higher purity would perform even better, but we take the lower number as our baseline, due to cost and availability.

#### B. Shielding

Figure 5 shows a proposed shielding configuration. There is an iron cube with walls 60 cm thick surrounding the source, and the gaps between the sleeve and this cube are also filled with iron. This is surrounded by a further 90 cm thick-walled cube of boron loaded concrete. These thicknesses were found

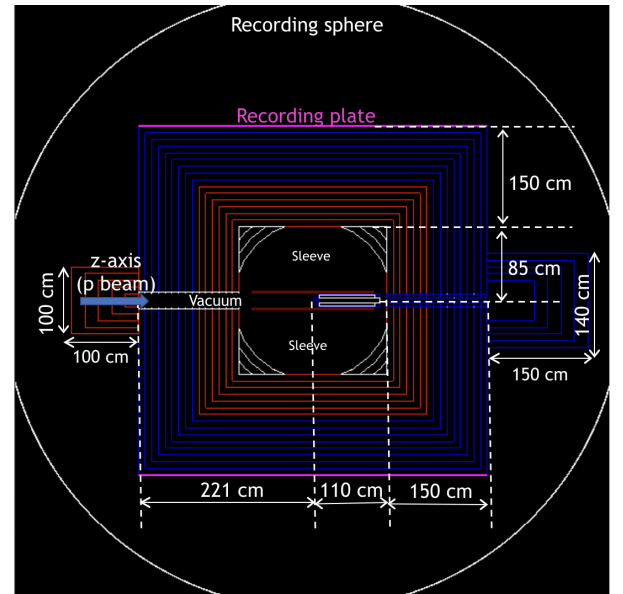


Fig. 5. Shielding around the IsoDAR target and sleeve.



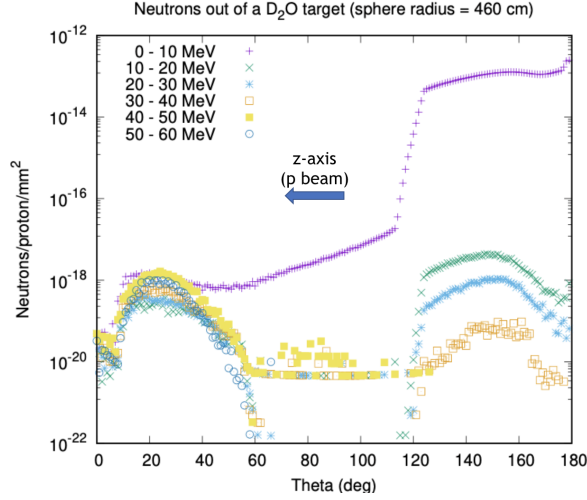


Fig. 6. Neutron flux emerging from the shielding, using a  $Be - D_2O$  target. The detecting sphere has a radius of 460 cm.

to be adequate in a previous study for the KamLAND site [4], and represent safe limits. There is a further concrete plug in the direction away from the beam entry (which points away from the detector), and a further iron block at the beam entry, which points towards the detector, representing the final bending magnet on the beamline. The outgoing neutron fluxes are recorded on a notional sphere of radius 460 cm around this system.

We now address a number of topics related to shielding and radiation levels in the experimental areas, presenting primarily the methodology for addressing these topics. As stated earlier, our calculations relate specifically to the Yemilab site, however they can be tailored to apply to any experimental site by inserting appropriate local conditions.

1) *Local Backgrounds*: Figure 6 shows the neutron flux resulting from the shielding arrangement in Figure 5, for various neutron energies, as a function of the angle  $\theta$  with respect to the proton direction. Units are neutrons per square mm (on the 460 cm notional sphere) per incident proton: to convert to the perhaps more familiar units of  $\text{cm}^{-2}\text{s}^{-1}$  they can be multiplied by  $6.24 \times 10^{18}$ .<sup>1</sup>

At high energies the neutrons peak in the forward direction, away from the detector. There is a comparatively large flux at large angles, heading towards the detector. These are low energy neutrons emerging from the back face, where the beam hits the target, and going backwards down the beam pipe, perhaps scattering a few times on the way. They are not stopped by the iron in the final bending magnet.

2) *Activation of components*: Activation of the accelerator components due to beam loss along the transport beam line and neutrons emerging from the target and shielding is a common problem for accelerators. However, another source of activation comes from neutrons emerging from the shielding. While beam loss can be addressed by careful optics, and controlled loss points along the beamline (collimators surrounded by good shielding), the background of neutrons from the shielding

cannot be so controlled. The principal activation problem will come from copper in the cables and magnet windings. To estimate the magnitude of this issue, simulations were done by placing a 1 cm thick Cu plate on the upper surface of the shielding block. Only gamma emitting isotopes with a lifetime longer than 24 hours were recorded in the simulation.

A radionuclide inventory shows that the isotopes that are the main contributors are  $^{64}\text{Cu}$ ,  $^{57}\text{Co}$ ,  $^{58}\text{Co}$ ,  $^{60}\text{Co}$  (Table I) although other isotopes like  $^{56}\text{Co}$ ,  $^{51}\text{Cr}$ , etc are also present but at much lower rates.

The activity of the Cu plate from this simulation is shown in Fig. 7. During beam on operation, additional radiation comes from beam loss (neutrons, gamma rays) or from electronic equipment (X-rays from RF amplifiers). However, when full operation is ongoing, no personnel will be allowed in the area. When the beam is off, there will be a small amount of radiation from activated material which, at least from neutrons emanating from the shielding, will be minimal after several days.

3) *Activation in the rock*: Some neutrons will escape the shielding during the experiment and will be absorbed in the rock causing rock activation. On completion of the experiment the resulting residual radiation must be low enough to enable the cavern to be open to other uses.

This depends not only on the escaping neutron flux but on the composition of the surrounding rock and also on the legal definition of “low enough”. We have compared a possible installation at Yemilab in Korea [24] with our previous study which assumed installation at KamLAND in Japan [25].

The regulation for the allowed rate at Yemilab is 10 Bq/g, a factor of 100 bigger than at KamLAND (0.1 Bq/g). An

| Isotope          | Half life | Isotope/proton    | Decay mode         |
|------------------|-----------|-------------------|--------------------|
| $^{64}\text{Cu}$ | 12 h      | $1.88\text{e-}16$ | $\beta^+, \beta^-$ |
| $^{57}\text{Co}$ | 270 d     | $2.25\text{e-}17$ | $\epsilon$         |
| $^{58}\text{Co}$ | 70 d      | $6.01\text{e-}17$ | $\beta^+$          |
| $^{60}\text{Co}$ | 1900 d    | $3.76\text{e-}17$ | $\beta^-$          |

TABLE I  
LIST OF THE MAIN RADIO-ISOTOPES INSIDE CABLES.

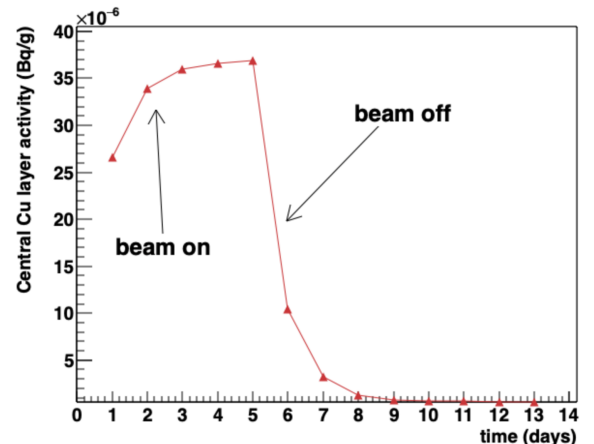


Fig. 7. Induced activity in a copper plate placed above the IsoDAR target, sleeve, and shielding block.

<sup>1</sup>A typical flux in a large power reactor is of order  $10^{13} \text{ n cm}^{-2} \text{ s}^{-1}$ .

| Compound                | Composition | Compound  | Composition |
|-------------------------|-------------|-----------|-------------|
| <b>CaCO<sub>3</sub></b> | 90%         | <b>U</b>  | 0.8 ppm     |
| <b>Na</b>               | 0.022%      | <b>Th</b> | 3.3 ppm     |
| <b>Co</b>               | 6 ppm       | <b>K</b>  | 11800 ppm   |
| <b>Eu</b>               | 0.2 ppm     |           |             |

TABLE II  
THE ROCK COMPOSITION AT YEMILAB.

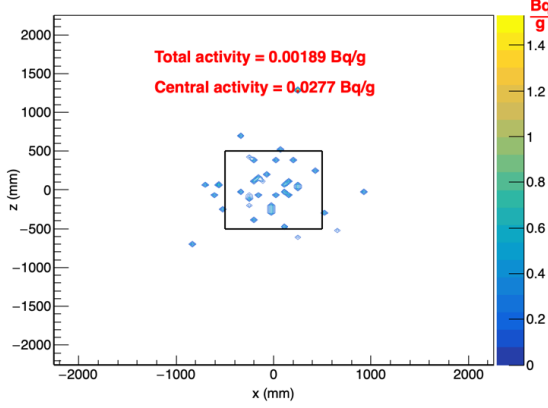


Fig. 8. Spatial distribution of induced activity in a rock layer in Bq/g.

assay of Yemilab rock showed that various types of rocks were found, limestone being the most abundant (almost 90% pure  $\text{CaCO}_3$ ) followed by quartz porphyry, pyrite and skarn minerals (silicate rocks which contain Ca, Fe, Mn, Al and Si minerals). Unlike the Inishi type rock found at KamLAND, the Yemilab environment is a factor of 10 lower in critical elements [low concentrations of Eu ( $< 1$  ppm), Co ( $< 10$  ppm) and more important Na (0.02%)]. The measured rock composition can be found in Table II.

The rock activation was estimated using the same technique as used for KamLAND [4] but with the Yemilab rock composition. The activation level is measured when the experiment is dismantled (about 4-5 years after the beam is turned off) and any rock activation of isotopes with half lives of less than one year or so would have totally decayed away. The long lived isotopes ( $\tau > 2-3$  years) like  $^{22}\text{Na}$ ,  $^{60}\text{Co}$  and the Eu pair present in the rock are activated by neutrons penetrating the rock.  $^{22}\text{Na}$  is produced by fast neutrons via the (n,2n) channel (11 MeV threshold), while the others are produced by thermal neutron activation. Table III shows a comparison between the abundance of the progenitor isotopes at KamLAND and Yemilab.

The simulations included a block of rock placed above the shielding with a 100 cm thickness to evaluate the induced

| Isotop            | Half life | Parent            | KamLAND | Yemilab |
|-------------------|-----------|-------------------|---------|---------|
| $^{22}\text{Na}$  | 2.6 y     | $^{23}\text{Na}$  | 6%      | 0.022%  |
| $^{60}\text{Co}$  | 5.3 y     | $^{59}\text{Co}$  | 30 ppm  | 6 ppm   |
| $^{152}\text{Eu}$ | 13.5 y    | $^{151}\text{Eu}$ | 3 ppm   | 0.1 ppm |
| $^{154}\text{Eu}$ | 8.6 y     | $^{153}\text{Eu}$ | 3 ppm   | 0.1 ppm |

TABLE III  
LONG LIVED ISOTOPES COMPARISON AT YEMILAB AND KAMLAND.

| Material | Yemilab (T/POT)       | KamLAND (T/POT)      |
|----------|-----------------------|----------------------|
| coolant  | $3 \times 10^{-5}$    | $11 \times 10^{-5}$  |
| sleeve   | $36.4 \times 10^{-3}$ | $1.7 \times 10^{-3}$ |

TABLE IV  
THE TRITIUM PRODUCTION IN THE YEMILAB AND KAMLAND  
TARGET/SLEEVE SYSTEMS.

activity at various depths in the rock. The total activity was calculated over the entire rock volume, however the highest activity concentration was measured on the central hot spot. Preliminary studies have shown that even for a shielding configuration consisting of 30 cm Fe and 90 cm of boron loaded concrete the highest central activity was less than 0.05 Bq/g (Figure 8). This is extremely low compared to the Korean legal requirement (10 Bq/g) and proves that rock activation at Yemilab is not an issue. This favourable result is due to several factors. First, the sodium concentration in the rock is very low, as is the concentration of Europium. In addition, the cobalt contamination in the rock is 5 times lower at Yemilab.

4) *Tritium production:* Tritium is produced in the target system in both the sleeve (by interaction of neutrons with Li) and heavy water coolant. It is a radiation hazard because of its long half life ( $\approx 12$  years) and the emission of beta particles. The tritium produced in the sleeve will remain trapped inside and will not be an issue, however the tritium produced in the coolant could be a problem because of potential leaks. It was found that the tritium produced in the heavy water with the Yemilab design is almost four times less than for the KamLAND version, and the exact values per incident proton in both materials are shown in Table IV. These differences result from changes in the target and sleeve geometries.

Tritium production could be a major issue in environments with difficult-to-control ground water in the experimental area. This was a serious issue at KamLAND, but fortunately is nonexistent at Yemilab, which is dry. Generally, mitigation of tritium generated in ground-water must be conscientiously addressed because of the difficulty in containment of this contaminant, and its potential for entering the local aquifers.

5) *Neutron Background in the detector:* Neutrons produced by proton interactions in the target system can be a background to analyses if they reach the detector. The analyses are likely to require a  $> 3$  MeV prompt signal to reduce confusion with neutron capture, but a fast neutron signal may be above this threshold. Neutron background can be reduced by pulse shape identification that discriminates between protons and electrons or positrons. Nevertheless, it is best to minimise the neutron rate into the detector rather than rely on cuts.

Ideally, the shielding to attenuate these neutrons should reduce the rate in the fiducial volume to below the naturally-occurring neutron level, which results from nuclear reactions induced by high-energy muons that reach the environment of the detector. To the best of our understanding, this is “a few neutrons per year (above 3 MeV) in the fiducial volume.” This represents, consulting the numbers shown in Fig. 10, an overall attenuation factor of about  $10^{-24}$ .

At KamLAND, the shielding consisted of a combination of

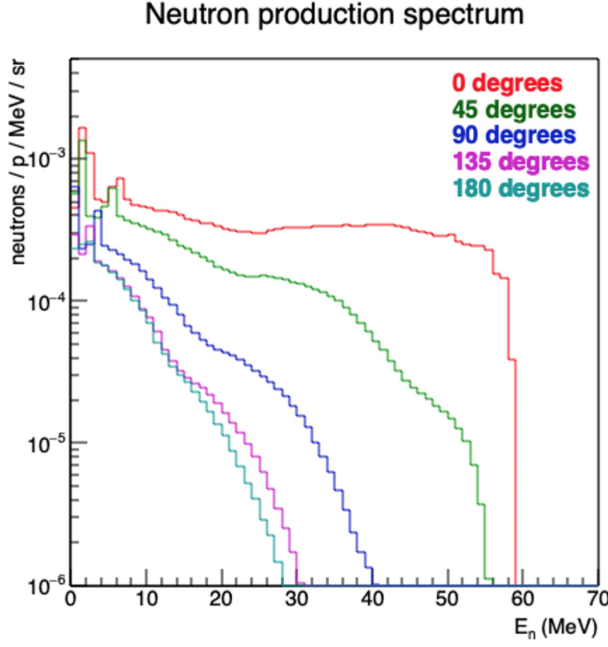


Fig. 9. Neutron spectra out of target for various angles.

2 m Fe and B-rich concrete placed around the target system with an extra 2 m length additional shielding of Fe towards the detector to further shield and prevent the neutrons from entering the detector [4]. While at KamLAND, the shielding design was constrained by the limited space of the cavern, this is not the case at Yemilab where the room that will accommodate the target and shielding system is quite large (a semicircular dome 7 m wide, 7 m tall and 22 m long). The energy spectra of the neutrons produced by the target for different angles with respect to the incident proton beam are shown in Figure 9. The backwards-going neutron flux is greatly reduced and this accounts for the target orientation as fast neutrons must not be allowed to reach the detector (note that the beam undergoes two 90° bends so that it hits the target while moving away from the detector).

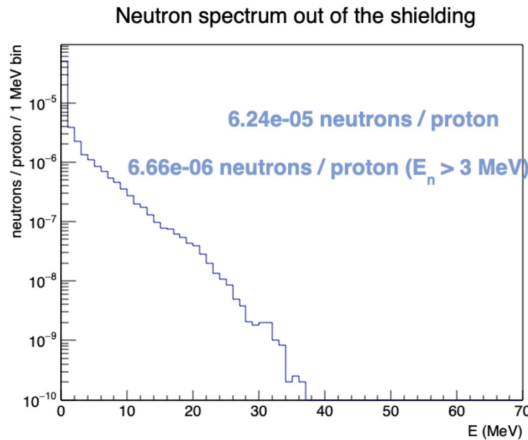


Fig. 10. Neutron spectra out of the beam pipe.

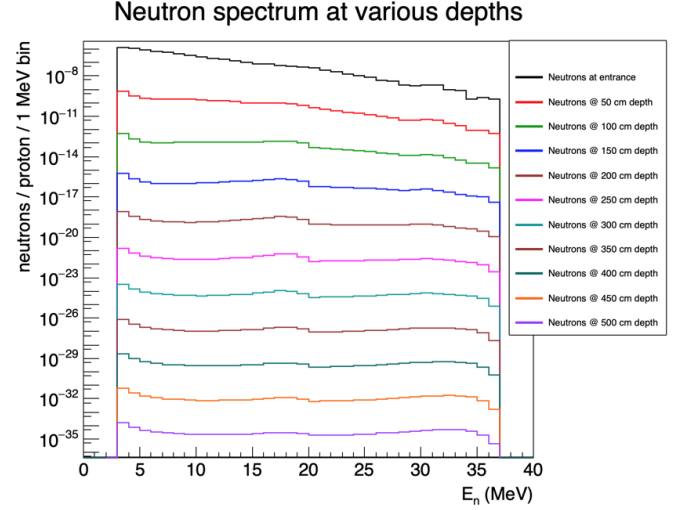


Fig. 11. Neutron spectra at various depths inside the shielding.

The energy spectra of the neutrons going through the vacuum pipe and emanating at the surface of the shielding in the backward direction is shown in Figure 10. To estimate the neutron background reaching the detector, these neutrons were tracked through an additional 5 metres thick iron block, since it is the fast (above 3 MeV) neutrons that can contribute to the additional background. Iron was the material of choice due to its high effective cross section for removing high energy neutrons. These neutrons spread out inside the block of iron, and their intensity is effectively attenuated.

The same technique used for KamLAND simulations, event biasing using particle splitting, was applied to evaluate the neutron flux towards the detector. However, the 5 metres of iron was far too great even when using these variance reduction techniques, and therefore this simulation was done in consecutive stages. The 5 metres block was divided into 10 layers, 50 cm thick. The energy spectrum and spatial distribution of neutrons were recorded at the end of each layer, and a new simulation was started using these values as input parameters for the following Fe layer. This has enabled the simulation of the entire thick block of iron. The energy spectra of the neutrons recorded after each iron layer are shown in Figure 11. The 3 MeV energy cut was applied in all these simulations.

After 5 m of Fe the neutron flux is reduced to  $\approx 10^{-35}$  neutrons/proton/MeV. This value is much lower than was obtained for the KamLAND shielding. The neutron attenuation in iron recorded in these simulations is shown in Figure 12.

6) *Photon background in the detector:* There will also be a background due to gamma rays, produced mainly by inelastic processes and also, at much lower rates, by neutron capture and subsequent isotopic decay. Photon inelastic processes and radioactive decay contribute even less. Other sources of photon background include beam loss along the transport line due to gas interactions or loss at collimators or the walls of the beam pipe.

This photon background is not relevant for the detection of  $\bar{\nu}_e$  particles through IBD events, again as these use the

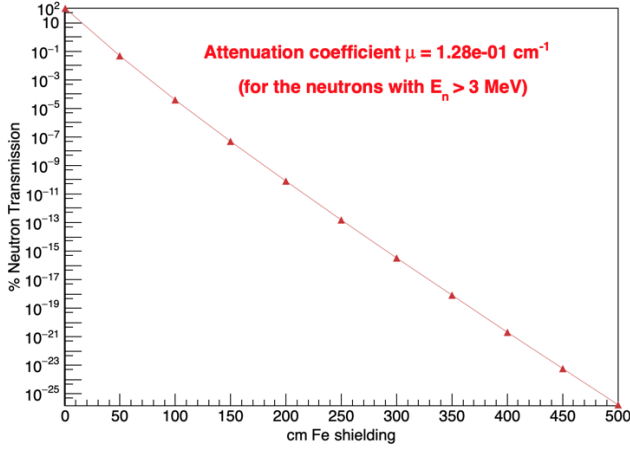


Fig. 12. Neutron transmission through the shielding.

“double flash” coincidence of the prompt positron and neutron capture events, but could in principle be a background for BSM searches which use a “single flash” signal from  $\bar{\nu}_e - e^-$  elastic scattering (ES).

Studies show [26] that the ES process has backgrounds from solar neutrinos and from IBD events with one of the ‘flashes’ undetected, with smaller contributions induced by cosmic rays and radiogenics. Mitigating these requires a visible energy threshold of 3 MeV, and a signal size of  $\sim 7000$  events (over 5 years running) is anticipated.

#### IV. DISCUSSION AND CONCLUSIONS

The design of the IsoDAR target and the sleeve has evolved, with increased understanding of the challenges of target design required to cool the 600 kW target in a confined space. As indicated, the engineering details will be presented in a separate publication. The simulations reported in this paper show that these challenges can be met without compromising the physics reach of the experiment, although high isotopic purity will be required for the lithium in the sleeve.

We report on the development of simulation tools to address a number of issues related to operating an experiment generating high levels of radiation in a low-background laboratory, specifically:

- 1) Optimisation of primary shielding design around the target
- 2) Activation of copper components
- 3) Tritium production
- 4) Activation of the rock
- 5) Neutron backgrounds in the detector
- 6) Photon backgrounds in the detector.

The results obtained give us confidence that such experiments can be successfully deployed without affecting the sensitivity of other experiments in the underground laboratory.

#### V. ACKNOWLEDGEMENTS

This work was supported by the US National Science Foundation through grants PHY-1912764 and PHY-1707969. DW was supported by the Heising-Simons foundation.

We are grateful to our colleagues from the Center for Underground Physics and Yemilab, in the Republic of Korea who have provided us with detail descriptions of the relevant conditions in their laboratory.

#### REFERENCES

- [1] J. Alonso, C. A. Argüelles, A. Bungau, J. M. Conrad, B. Dutta, Y. D. Kim, E. Marzec, D. Mishins, S. H. Seo, M. Shaevitz, J. Spitz, A. Thompson, L. Waites, and D. Winklehner. Neutrino physics opportunities with the IsoDAR source at Yemilab. *Physical Review D*, 105(5):052009, 3 2022. Publisher: American Physical Society.
- [2] Daniel Winklehner. IsoDAR@Yemilab—A Definitive Search for Noble Neutrinos and Other BSM Physics. *Physical Sciences Forum*, 8(1):21, 2023. Number: 1 Publisher: Multidisciplinary Digital Publishing Institute.
- [3] J. R. Alonso, J. M. Conrad, D. Winklehner, J. Spitz, L. Bartoszek, A. Adelmann, K. M. Bang, R. Barlow, A. Bungau, L. Calabretta, Y. D. Kim, D. Mishins, K. S. Park, S. H. Seo, M. Shaevitz, E. A. Voirin, and L. H. Waites. IsoDAR@Yemilab: A report on the technology, capabilities, and deployment. *Journal of Instrumentation*, 17(09):P09042, 9 2022. Publisher: IOP Publishing.
- [4] Adriana Bungau, Jose Alonso, Larry Bartoszek, Janet M. Conrad, Edward Dunton, and Michael H. Shaevitz. The shielding design concept for the isodar neutrino target. *Journal of Instrumentation*, 15(07):T07002, jul 2020.
- [5] A. Bungau, J. Alonso, L. Bartoszek, J. Conrad, M. Shaevitz, and J. Spitz. Optimizing the  $^8\text{Li}$  yield for the IsoDAR neutrino experiment. *Journal of Instrumentation*, 14(03):P03001–P03001, mar 2019.
- [6] Daniel Winklehner, Jose R. Alonso, and Janet Conrad. A new family of high-current cyclotrons for isotope production. *Journal of Radioanalytical and Nuclear Chemistry*, June 2024.
- [7] Daniel Winklehner, Janet M. Conrad, Devin Schoen, Maria Yampolskaya, Andreas Adelmann, Sonali Mayani, and Sriramkrishnan Muralikrishnan. Order-of-magnitude beam current improvement in compact cyclotrons. *New Journal of Physics*, 24(2):023038, 2 2022. Publisher: IOP Publishing.
- [8] Seon-Hee Seo et al. Physics Potential of a Few Kiloton Scale Neutrino Detector at a Deep Underground Lab in Korea. *arXiv*, 9 2023.
- [9] F. Kaether, W. Hampel, G. Heusser, J. Kiko, and T. Kirsten. Reanalysis of the GALLEX solar neutrino flux and source experiments. *Phys. Lett. B*, 685:47–54, 2010.
- [10] J. N. Abdurashitov et al. Measurement of the solar neutrino capture rate with gallium metal. III: Results for the 2002–2007 data-taking period. *Phys. Rev. C*, 80:015807, 2009.
- [11] V. V. Barinov et al. Search for electron-neutrino transitions to sterile states in the BEST experiment. *Phys. Rev. C*, 105(6):065502, 2022.
- [12] C. Athanassopoulos et al. Results on  $\nu_\mu \rightarrow \nu_e$  neutrino oscillations from the lsnd experiment. *Phys. Rev. Lett.*, 81:1774–1777, Aug 1998.
- [13] MiniBooNE Collaboration, A. A. Aguilar-Arevalo, B. C. Brown, J. M. Conrad, R. Dharmapalan, A. Diaz, Z. Djuricic, D. A. Finley, R. Ford, G. T. Garvey, S. Gollapinni, A. Hourlier, E.-C. Huang, N. W. Kamp, G. Karagiorgi, T. Katori, T. Kobilarcik, K. Lin, W. C. Louis, C. Mariani, W. Marsh, G. B. Mills, J. Mirabal-Martinez, C. D. Moore, R. H. Nelson, J. Nowak, I. Parmaksiz, Z. Pavlovic, H. Ray, B. P. Roe, A. D. Russell, A. Schneider, M. H. Shaevitz, H. Siegel, J. Spitz, I. Stancu, R. Tayloe, R. T. Thornton, M. Tzanov, R. G. Van de Water, D. H. White, and E. D. Zimmerman. Updated MiniBooNE neutrino oscillation results with increased data and new background studies. *Physical Review D*, 103(5):052002, 3 2021. Publisher: American Physical Society.
- [14] Loyd Waites, Adrian Thompson, Adriana Bungau, Janet M. Conrad, Bhaskar Dutta, Wei-Chih Huang, Doojin Kim, Michael Shaevitz, and Joshua Spitz. Axionlike particle production at beam dump experiments with distinct nuclear excitation lines. *Phys. Rev. D*, 107(9):095010, 2023.
- [15] Matheus Hostert, David McKeen, Maxim Pospelov, and Nirmal Raj. Dark sectors in neutron-shining-through-a-wall and nuclear-absorption signals. *Phys. Rev. D*, 107(7):075034, 2023.
- [16] T Koi. A Geant4 physics list for shielding calculations, 2010.
- [17] D H Wright and M H Kelsey. The Geant4 Bertini cascade, 2015. Publisher: Nuclear Instruments and Methods in Physics Research Section A: Accelerators, Spectrometers, Detectors and Associated Equipment, 804:175 – 188.
- [18] C Gulliford N MacFadden, S Peggs. Development and validation of a Geant4 radiation shielding simulation framework, 2018.

- [19] OECD. Shielding aspects of accelerator, targets and irradiation facilities, 2014. Publisher: Workshop Proceedings, Tsukuba, Japan, Nuclear Science, OECD Publishing, Paris.
- [20] Hirayama. Inter-comparison of the medium-energy neutron attenuation in iron and concrete, 1997. Publisher: Proceedings of the SATIF-3, Shielding Aspects of Accelerators, Targets and Irradiation Facilities, Tohoku University, pp. 185-195.
- [21] T. Rinckel, D.V. Baxter, J. Doskow, P.E. Sokol, and T. Todd. Target performance at the low energy neutron source. *Physics Preocedia*, 26:168–177, 2012.
- [22] J. Allison et al. Recent developments in Geant4. *Nucl. Instr. & Meth. A*, 835:186–225, 2016.
- [23] J. Chadwick. Possible existence of a neutron. *Nature*, 129:312, 1932.
- [24] K.S. Park et al. Construction of Yemilab. *Frontiers in Physics*, 12:1323991, 2024.
- [25] M. Abs et al. IsoDAR @ KamLAND: a conceptual deisgn report for the technical facility. <https://arxiv.org/abs/1511.05130>, 2015.
- [26] J. R. Alonso et al. Neutrino physics opportunities with the isodar source at yemilab. <https://arxiv.org/abs/2111.09480>.